Article

Analysis of Deformation in an Aluminium Hull Impacting Water Free Surface

Alessandro Mercuri [1], Pierluigi Fanelli [1], Giacomo Falcucci [2,3], Stefano Ubertini [1,*], Elio Jannelli [4] and Chiara Biscarini [5]

[1] Department of Economics, Engineering, Society, and Business Organisation, University of Tuscia, 01100 Viterbo, Italy; alessandro.mercuri@unitus.it (A.M.); pierluigi.fanelli@unitus.it (P.F.)
[2] Department of Enterprise Engineering "Mario Lucertini", University of Rome "Tor Vergata", 001133 Roma, Italy; giacomo.falcucci@uniroma2.it
[3] Department of Physics, Harvard University, Cambridge, MA 02138, USA
[4] Department of Engineering, University of Naples "Parthenope", 80143 Napoli, Italy; elio.jannelli@uniparthenope.it
[5] UNESCO Chair in Water Resources Management and Culture, University for Foreigners of Perugia, 06125 Perugia, Italy; chiara.biscarini@unistrapg.it
[*] Correspondence: stefano.ubertini@unitus.it

Abstract: Water impacts provide a challenge for a wide range of applications, from aerospace, to marine, mechanical and civil engineering, due to the complexity conveyed by the coexistence of impulsive loads, large local deformations and high-amplitude vibrations. Thus, the need for reliable structural health monitoring (SHM) systems is emerging in the industrial field of fluid-structure interaction (FSI) applications. In this paper, we leverage the previous work on strain and displacement fields reconstruction to analyse a scale aluminium model subject to water vertical and oblique impacts. Fibre Bragg grating (FBG) sensors were installed on the hull ribs and used both as reconstruction sensors (to reconstruct the structure mechanical behaviour characteristics) and as control sensors, by using their signals to compare the real and reconstructed structural parameters, at the sensors locations. Finally, the effectiveness of different reconstruction layouts was investigated referring to the strain signal reconstruction quality in case of both vertical and oblique impacts. Results show the potential of the described method for the reconstruction of strain signal through a proper choice of the reconstruction sensors positions both in case of vertical and oblique impacts.

1. Introduction

An effective understanding of fluid-structure interaction phenomena represents an essential requirement to face the design of tools for mechanical, marine and civil industrial applications; this leads to a large presence of this topic in the scientific literature [1–3]. In particular, the water impact of solid bodies triggers the onset of hull slamming phenomena, whereby large, impulsive forces are applied to the structure, with the consequent presence of vibrations, local buckling and deformation events. Thus, these phenomena play a key role both in the design and in the maintenance of structures interacting with the water free surface, e.g., ships hulls, fuselages or rockets [1–4]. Furthermore, effective and reliable tools for the real-time monitoring of impulsive loads, structural response and possible damages are required for industrial applications: at the moment, current solutions are still under development from a scientific and a technological point of view [4]. An experimental methodology for the reconstruction of the structural behaviour of solid bodies (i.e., strain and displacement fields) from discrete local strain measurements in case of free

water surface impact has been presented by some of the authors in previous works [5–8]. More specifically, local strain measurements from Fibre Bragg grating (FBG) sensors in a distributed network were used as the input to reconstruct the strain field and the deformed shape of compliant bodies. Furthermore, this method has been tested for damage detection purposes, through a numerical analysis on cylinders affected by delaminations in several locations [6]. The potential of such a methodology for structural monitoring has been proved in [9–13] as well, for the detection and localization of structural failures typically related to hull slamming phenomena. FBG sensors were chosen due to their high sensitivity (also in the case of high-frequency dynamic systems), which is not affected by their employment in water environment or in the presence of noise sources (e.g., electromagnetic noise). Moreover, FBG sensors can be arranged in arrays built within a single optical fibre, allowing synchronous data acquisition in several locations [14–19].

In this paper, we employ the aforementioned methodology to the structural behaviour reconstruction of wedges, the reference geometry for ship hull bottom. Bodies' impact on free water surface represents an interesting and widely investigated topic in the literature, in particular in the case of cylindrical bodies [20–30] and wedges [31,32]. These works are mainly focused on fluid dynamics, on the evolution of the free surface and the pile-up [26–29] through both numerical and experimental analyses [21,24,32]; moreover, some works concern fluid-structure interaction considering both rigid and flexible structures and several levels of complexity, from simple systems (in terms of structure geometry and fluid-structure interaction) [23,25,31] to advanced applications concerning sea loads on simple geometries [22] or complex geometries [20,30]. Here the proposed reconstruction methodology [6] is applied to a three-dimensional aluminium wedge modified as a ship hull. First, we aim at reconstructing the strain field of the body impacting the free surface from different angles, by using local strain signals from reconstruction sensors. Second, we show that the comparison between reconstructed and effective strain signals from control sensors in correspondence with control sensors locations provide an accurate control on reconstruction results; the goal is a strain reconstruction which is as close as possible to the real-one, to compare these results with the damage-influenced ones in future works and check for the effectiveness of the methodology for structural health monitoring purposes in case of relevant differences between reconstructed values for damaged and undamaged structures. Finally, an analysis of sensors positions choice is presented, focusing on the effects on the reconstruction results of the changing of reconstruction and control sensors positions within the same FBGs measurement system. The paper is organized as follows. Section 2 shows the experimental setup and its main features. Section 3 describes the reconstruction method. Section 4 is dedicated to the presentation of the numerical model of the wedge. Results are discussed in Section 5, before the Discussion section and the conclusions.

2. Experimental Setup

The experimental setup has been designed to allow water impact tests at different impact angles. Tests are carried out in a tank (length 1.85 m, width 1.98 m, height 0.81 m) realized with a stainless-steel frame with plexiglass panels, with water level set to 0.48 m. The water impact setup includes an aluminium rail and a carriage system, consisting of a slender and specimen attach system. In particular, the sledge and the rail can be rotated to modify the V angle (between the vertical direction and the specimen velocity vector, controlled through the rail inclination as depicted in Figure 1a,b, while a junction in correspondence with the specimen attachment system allows the variation of the G angle (the angle between the wedge symmetry axis and the normal to the water surface, see Figure 2b). The experimental setup is depicted in (Figure 1b). Wedge vertical position is measured through three SpectraSymbol® Thinpot® (SpectraSymbol, Salt Lake City, UT, USA) linear potentiometers, positioned along the rail. The FBGs signals are synchronously acquired through a National Instruments® NI-USB-6009 (National Instruments, Austin, TX, USA). FBGs have been chosen for strain measurements during the impact tests. They

consist of gratings characterized by a modified refractive index compared to that of the optical fibre core [14]; this perturbation causes the reflection of light which propagates along the fibre within a range of wavelengths. Referring to the Bragg condition, reflection bandwidth values depend on the grating period and the refractive index, i.e., strain and temperature variations cause modifications in grating period and, consequently, in reflected bandwidth, which represents FBGs output signal to be converted in strain and temperature values knowing original reflected bandwidth. FBG sensors have been chosen because of their high sensitivity, also in the case of high-frequency dynamic systems [15,16], for the low sensitivity to water and noise sources (e.g., electromagnetic noise) and for the possibility of using arrays of sensors built on a single optic fibre, allowing synchronous data acquisition in several locations. These features make FBGs reliable strain sensors in the case of water impact tests [14–19]. Moreover, optical fibres do not interfere with body structural behaviour in terms of added mass or modifications in strength of stiffness, because of their lightness, small size and high flexibility; they can be easily integrated into the structure and, in case of composite bodies, embedded in the structure itself. The FBG network is made of 12 grating sensors attached onto the wedge rib through epoxy glue, both on hull model rib top (sensors 1–6) and bottom (sensors 7–12). To be noted, the locations of the upper and lower rows of sensors are not aligned. Sensor positions are reported in Figure 3 Sensors Bragg wavelengths (λ_B) and their wavelengths are summarized in Table 1.
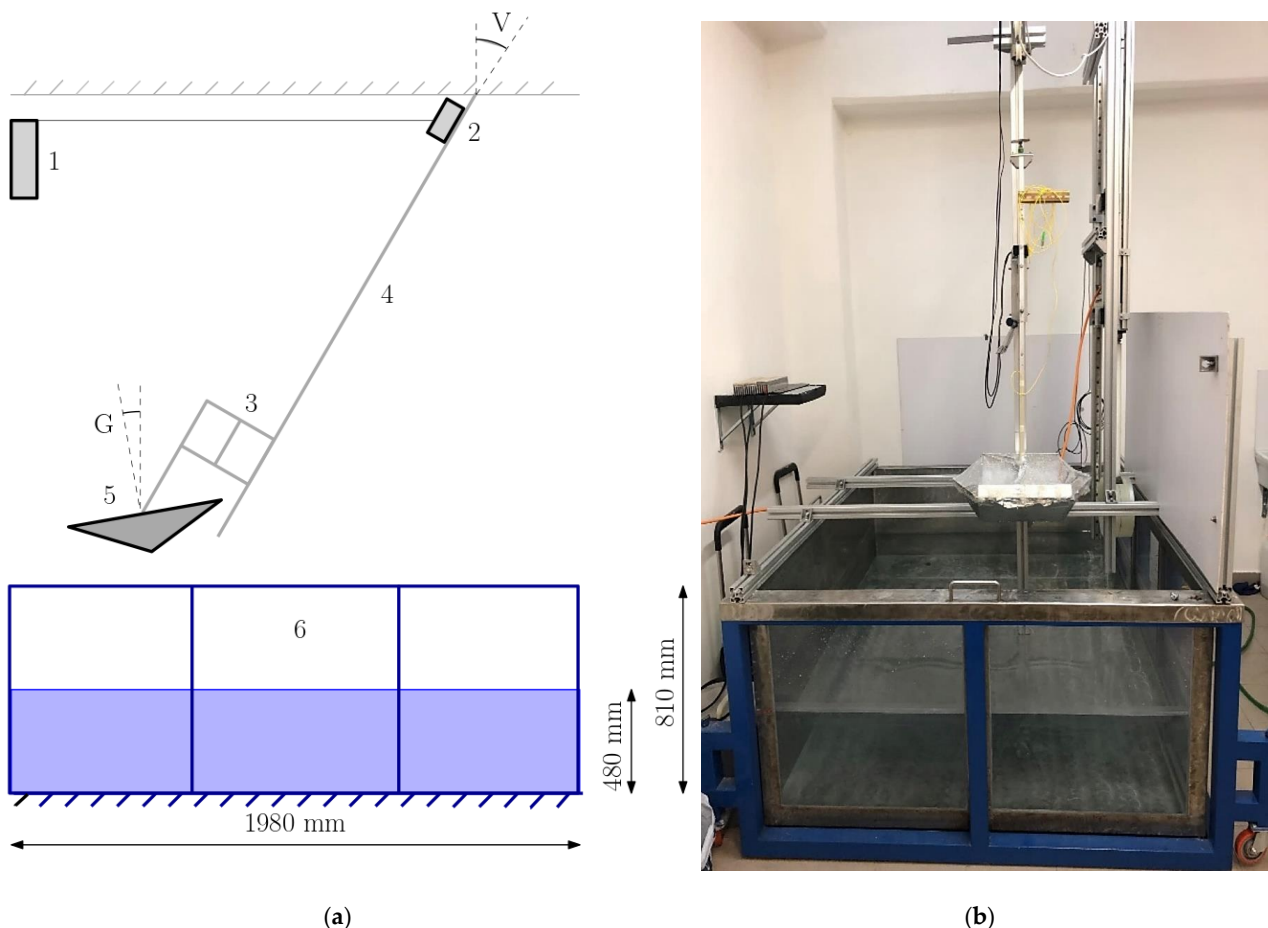

Figure 1. (**a**) Scheme of the experimental setup: 1—Data acquisition system. 2—FBG connector. 3—Carriage system. 4—Rail. 5—Specimen. 6—Water tank. (**b**) Lateral view of the experimental setup.
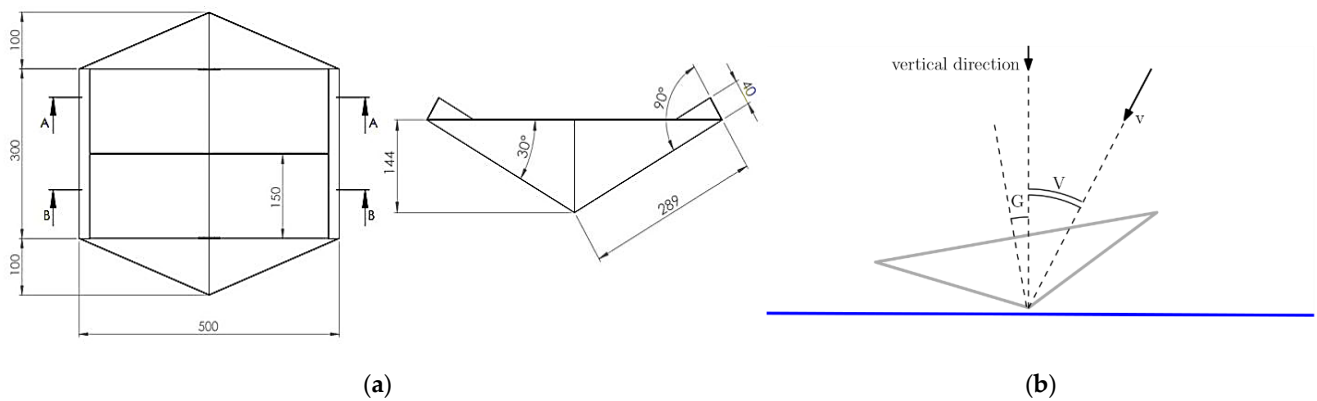
(**a**)

(**b**)

Figure 2. (**a**) Specimen geometry and dimensions. (**b**) V and G angles scheme.
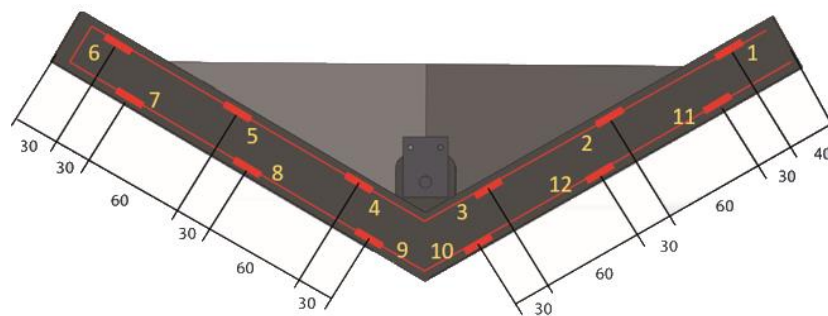
Figure 3. FBG sensors positions on specimen rib.

Table 1. Sensors Bragg wavelengths (λ_B).

Sensor	λ_B [nm]	Sensor	λ_B [nm]
1	1531.03	7	1548.99
2	1534.07	8	1552.10
3	1537.07	9	1555.06
4	1540.13	10	1557.99
5	1542.98	11	1561.11
6	1545.93	12	1564.22

The FBG interrogation system used during the experimental tests can operate with a maximum sampling frequency of 3 kHz. Such a system is made of a laser source, characterized by an average optical power output of 3 mW and a bandwidth of 80 nm. System repeatability is ±3 pm, while the strain resolution is around 1 pm. The wedge is made of aluminium (modulus of elasticity (E) 70 GPa, Poisson ratio (ν) 0.33, density (ρ) 2700 kg/m³), with a 0.5 m length, 0.5 m width and 0.144 m height; the aluminium plate which acts as hull bottom has a 30° deadrise angle.

A thin aluminium plate, which acts as the rib of a ship hull, is welded at the centre of the wedge bottom. Two plates are welded on hull bottom edges, to fix the specimen to the sledge through a steel beam and two other plates are fixed to the sledge itself (Figure 2a).

3. Shape Reconstruction Methodology

The reconstruction of the strain and the displacement fields of the wedge was based on the modal decomposition approach, following the analytical procedure described in previous works [12,13]. The mechanical behaviour of the body, both in terms of strain and displacement, was obtained through a discrete number of mode shapes. Modal coordinates

$\mu(t)$ described the elastic response of the wedge; the knowledge of modal coordinates over time allows the computation on strain vector $\varepsilon(t)$ and displacement vector $w(t)$:

$$w(t) = \Phi \, \mu(t) \tag{1}$$

$$\varepsilon(t) = \Psi \, \mu(t) \tag{2}$$

where Φ and Ψ are N × M matrices, collecting modal displacement and modal strain normalized components at the measurement locations (N is the number of measurement locations and M the number of mode shapes), $w(t)$ and $\varepsilon(t)$ are the time-dependent displacements ($w_n(t)$) and strains ($\varepsilon_n(t)$), respectively, at the measurement location n. Matrices Φ and Ψ are characteristics of the body and can be obtained analytically, numerically or experimentally once before reconstruction, consequently, they require no updates in absence of modifications on the structure or damages.

For reconstruction purposes, modal coordinates can be computed at each timestep from the strain values measured by FBG sensors as:

$$\mu(t) = \left(\Psi^T \, \Psi \right)^{-1} \Psi^T \, \varepsilon(t) \tag{3}$$

being $\mu(t)$ the modal coordinates vector gathering the $\mu_m(t)$ of each mode over time. The reconstruction of the overall deformation can be achieved with the substitution of matrix Φ with matrix φ gathering the normalized modal displacements at the required locations. The specimen analysed here consisted of a ship hull model based on a wedge; the gathering of φ and Ψ matrices requires a numerical modal analysis. Substituting Equation (3) in Equations (1) and (2), displacements $w(t)$ and strains $\varepsilon(t)$ can be computed as:

$$w(t) = \varphi \, (\Psi^T \, \Psi)^{-1} \Psi^T \, \varepsilon(t) \tag{4}$$

$$\varepsilon(t) = \Psi \, (\Psi^T \, \Psi)^{-1} \Psi^T \, \varepsilon(t) \tag{5}$$

More details on this procedure are available in [5,6].

4. Numerical Model

The gathering of Φ and Ψ matrices provides a modal analysis of the ship hull model, based on the finite element (FE) model of the specimen (see Figure 4. FE model of the specimen). The components realized with an aluminium sheet, such as hull bottom, rib and support plates, were modelled as eight-node shell elements with six DOF for each node and bending and membrane stiffness. The steel beam used to link the sledge plates and the hull plates (or central and lateral plates) was modelled as a 3D two-node beam element with six DOF for each node. The model also included welds, modelled through contact pairs made of target elements on the rib and contact elements on the hull bottom; contact is modelled as bonded.

Referring to the features of the wedge attachment system, a fixed support constraint was adopted for all the central plates nodes. The modal analysis was performed to extract the first hundred normalized shape modes. Considering their effectiveness for reconstruction purposes, especially in correspondence with the hull rib, eight modes were chosen to gather both Φ matrix and Ψ matrix (Table 2). Mode shapes chosen for reconstruction and their frequencies); for the first one, displacement values in correspondence with sensors, we collected positions for all the six degrees of freedom, while, for the Ψ matrix, strain values on the same positions were chosen.

Table 2. Mode shapes chosen for reconstruction and their frequencies.

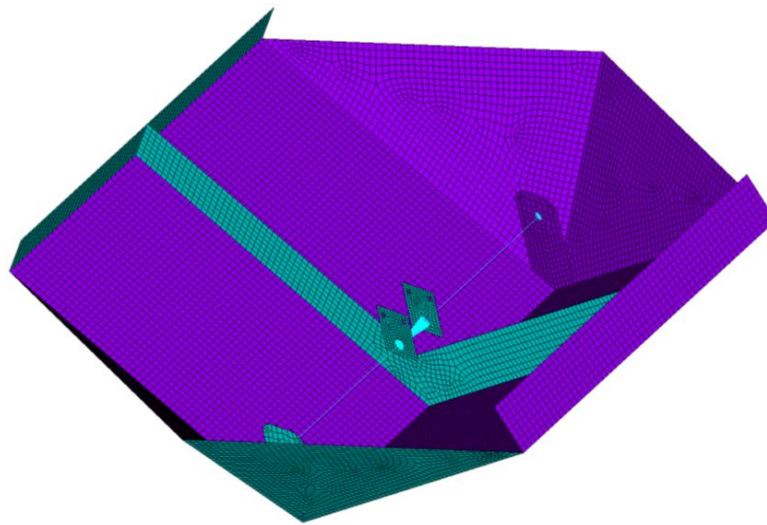| Mode Shape	69	70	71	74	78	83	86	89
Frequency [Hz]	715.3	721.8	725.9	763.7	827.7	902.6	921.1	949.1

Figure 4. FE model of the specimen, characterized by 14,315 elements and 42,155 nodes.

5. Results

The experiments were carried out through the experimental setup and specimen described in the previous sections, by realizing several water impact tests characterized by the same drop height (0.5 m) and different V and G impact angles. Experimental tests features are summarized in Table 3.

Table 3. Experimental tests features.

| Specimen	Drop Height	Impact Angles
Al wedge	0.5 m	0° V/0° G 0° V/10° G 10° V/0° G

Twelve sensors were attached to the hull rib (see Figure 3) to measure the local strain during the test. The sampling frequency was 2500 Hz; for reconstruction and evaluation purposes, reconstruction sensors and control sensors were identified. Reconstruction sensors signals were used for the reconstruction of the displacement field and strain field (Equations (4) and (5)) on the structure. Control sensors allow the computation of the reconstruction error, by comparing reconstructed and effective strain signals in correspondence with their location as follows:

$$E_n = \frac{\sum_{k=1}^{K} \left| \frac{[\bar{\varepsilon}_n(k) - \varepsilon_n(k)]}{K} \right|}{max(|\bar{\varepsilon}_n(k)|)} \qquad (6)$$

where $\bar{\varepsilon}_n(k)$ and $\varepsilon_n(k)$ are the n-sensor measured and reconstructed strains at the k-th timestep and K is the total number of time samples collected during the experimental test. Referring to previous studies' results and considering the introduction of E_n as a new reconstruction parameter, an error value lower than 0.15 can be considered as acceptable and the reconstruction method—remembering the analysed reconstruction layouts—can be considered validated. The choice of reconstruction sets influences the reconstruction quality and, consequently, the E_n value. For this reason, we opted to consider three different reconstructions of eight sensors with different characteristics; consequently, four control sensors were used to assess the reconstruction quality through the E_n parameter computed at each control location. The aforementioned mode shapes were chosen considering their influence on the structural behaviour of the hull rib, i.e., the location of both the reconstruction and the control sensors. Moreover, reconstruction

sensors were chosen in order to avoid nodes with zero strain locations on the structure (mode nodes), which could lead to reconstruction errors.

Reconstruction layouts are presented in Figure 5. Layout 1 (L1) is characterized by the choice of reconstruction sensors positioned on the top and on the bottom left of the rib, in order to achieve a good reconstruction quality and to concentrate control sensors on the rib bottom right (with the exception of sensor 8). Layout 2 (L2) is similar to L1, but control sensors have been equally distributed between left and right rib bottom, to achieve a more complete control and, reconstructing from both left bottom and right bottom placed sensors, a higher-quality reconstruction. In Layout 3 (L3) a top placed control sensor was chosen to extend the reconstruction quality control on this part of the rib. Moreover, the sensors' locations reflect the need for avoiding strain signal from sensors placed near welding points and for preferring signal from sensors placed near modes' strain maximum. Results are presented as comparisons between reconstructed and measured strain signal and as E_n values tables to resume the quality of the reconstruction for each layout and test.
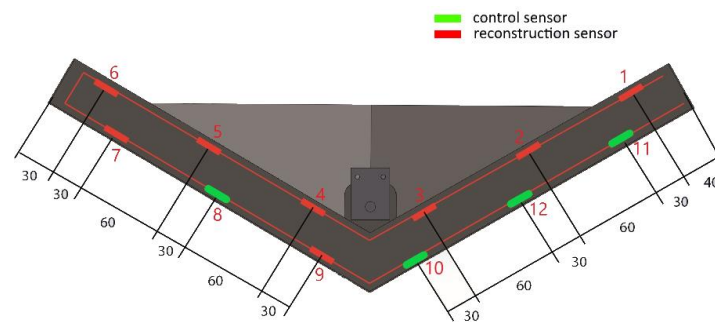
(**a**) Layout 1
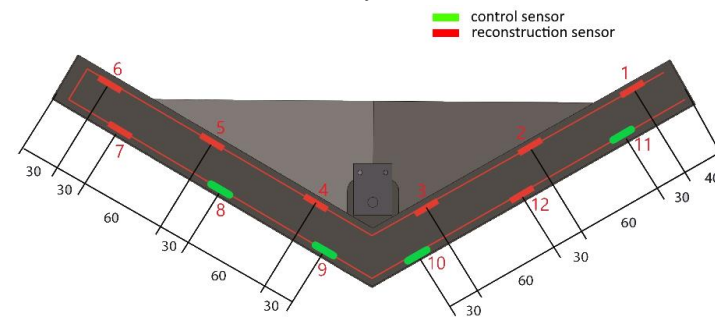
(**b**) Layout 2
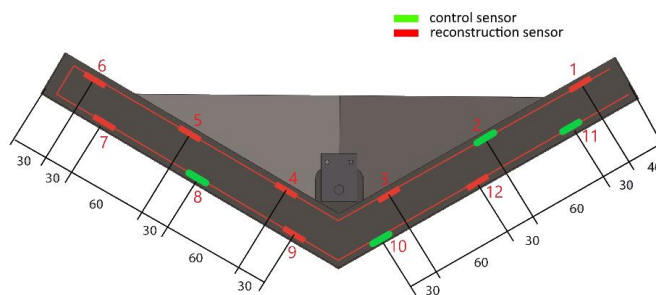
(**c**) Layout 3

Figure 5. Reconstruction sensors and control sensors position for analysed (**a**) Layout 1, (**b**) Layout 2, (**c**) Layout 3. Green marks and red marks represent control sensors and reconstruction sensors respectively.

5.1. 0° V–0° G Impact (Vertical Impact)

The first experimental test consists of an 0° V–0° G impact (i.e., a perfect vertical impact), considering a drop height of 0.5 m. Results in terms of reconstructed and measured strain signal for the four control sensors of each layout are presented in (Figures 6–8), while the error values for control sensors are listed in Table 4. Results from Layout 1 show a good agreement between reconstructed and measured signals. Referring to Figure 6 it is clear how the reconstructed signals match the measurements in terms of frequency and, in most of the cases, signal amplitude (see sensor 11 results, for example). Sensor 10 shows the worst results among all; comparing measured and reconstructed signals it is clear that the reconstruction is acceptable in terms of frequency and strain signal, while the reconstructed amplitude is far from the measured one. This could be related to the position of sensor 10, which was near to the keel and, therefore, subject to the impact pressure before all the other hull positions; in fact, the amplitude gap between measured and reconstructed signal tends to reduce after the beginning of the impact (see the first timesteps). Layout 2 shows an appreciable performance in terms of reconstruction (Figure 7). Both reconstructed and measured signals in sensors 9 (chosen as a reconstruction sensor in Layout 1) and 11 do not differ much, in particular during the first part of the impact. For Layout 2, sensor 10 signals show the before exposed characteristics related to the sensor location. Layout 3 does not feature appreciable differences in reconstruction output if compared with the others; it is worth noting that the reconstruction on sensor 2's position shows higher peaks than the measured signal but the same frequency (Figure 8).
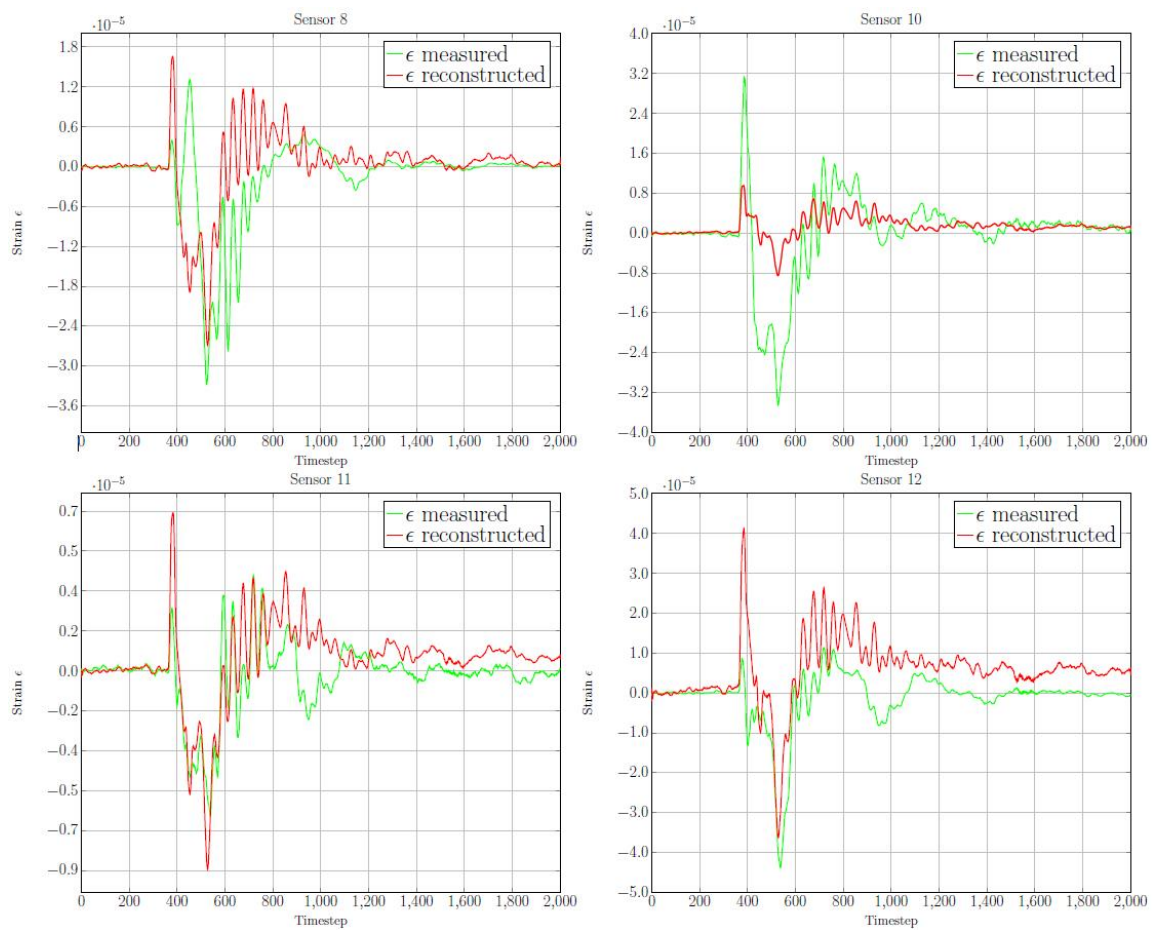

Figure 6. 0° V–0° G impact test—Layout 1 measured vs. reconstructed strain signals.

Figure 7. 0° V–0° G impact test—Layout 2 measured vs. reconstructed strain signals.

Table 4. 0° V–0° G impact test—Layout reconstruction errors E_n for each control sensor.

Layout	Control Sensors	Error on CS 1	Error on CS 2	Error on CS 3	Error on CS 4
L1	8-10-11-12	0.113	0.126	0.153	0.151
L2	8-9-10-11	0.117	0.110	0.143	0.095
L3	2-8-10-11	0.132	0.106	0.132	0.096

Table 3 shows results in terms of reconstruction errors; E_n values are generally good, except for sensors 10 and 11 position for the first layout, related to the difference in first peaks values between measured and reconstructed signals. The best reconstruction performances can be attributed to Layouts 2 and 3, which are designed to have the most homogeneous distribution on reconstruction sensors, in particular for those positions far to the keel (e.g., sensor 11 position), considering that the computation of modal coordinates from strain signals measured in locations which are not so far from the control positions helps in achieving an higher-quality reconstruction; on the other hand, Layout 3 offers an appreciable reconstruction near to the keel, thanks to the presence of sensor 9, which is near to the keel, in the reconstruction set. This allows a better computation of modal coordinates, considering the higher stiffness of the structure in correspondence with the keel itself. Taking into account the above-investigated features of the reconstruction on the positions near to the keel, especially during the impact, it is interesting to extend the analysis to oblique impacts, to understand the importance of the water entry both in terms of specimen velocity inclination and the wedge orientation (i.e., V and G angles).
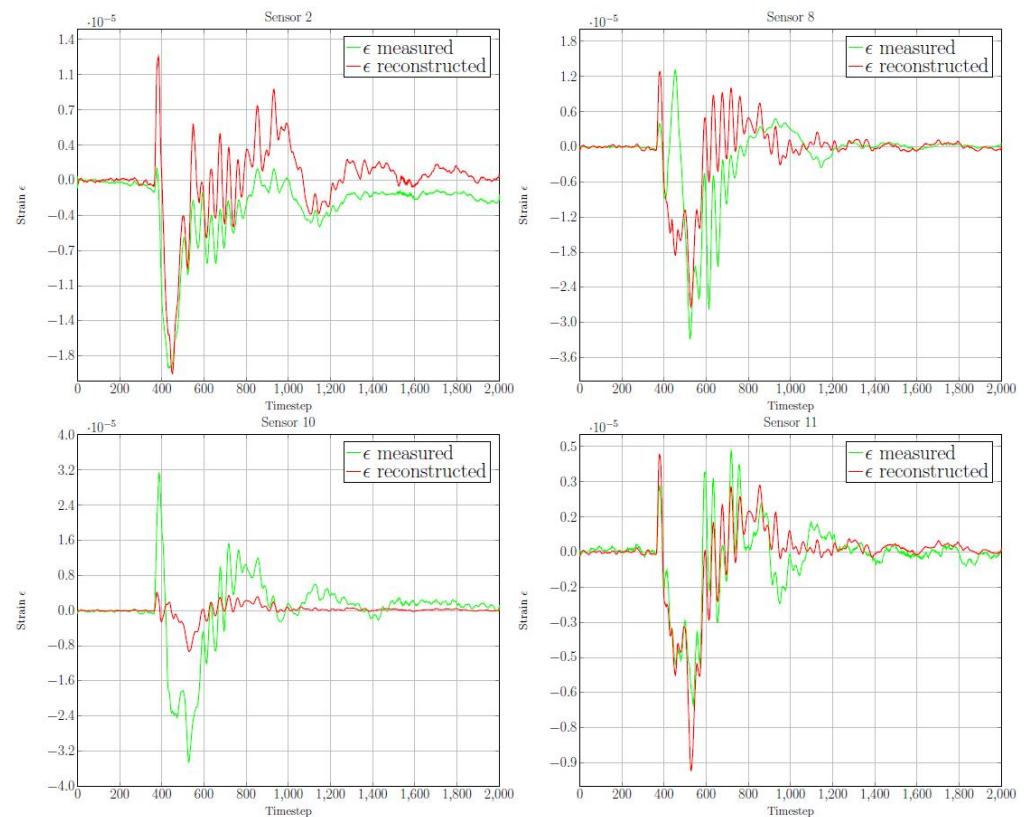
Figure 8. $0°$ V–$0°$ G impact test—Layout 3 measured vs. reconstructed strain signals.

5.2. $0°$ V–$10°$ G Impact

The second impact test is characterized by a $0°$ V–$10°$ G impact angle, set through an anticlockwise rotation of the wedge in correspondence with the attachment joint, and drop height of 0.5 m. Reconstructed and measured strain signals of the four control sensors of each layout are shown in Figures 9–11. Table 5 resumes the E_n error values for the same sensor positions. Results referred to L1 reconstructed and real signals on control sensor positions feature the reconstruction goodness in terms of frequency and signal amplitude; on the other hand, sometimes measured and reconstructed peaks do not coincide in time. For this test, sensor 10 position shows the worst comparison between measured and reconstructed signal; nevertheless, although the reconstruction error is lower with respect to the previous test, this confirms that the water entry dynamics related to the impact angle has an effect on the reconstruction effectiveness. L2 substantially features the same reconstruction performance as L1. As for the $0°$ V–$0°$ G test, sensors 9 and 11 reconstructed and measured signals show appreciable performances in the beginning of the impact; moreover, sensors 8 and 10 feature a lower quality reconstruction, especially after the impact. L3 is characterized by a good reconstruction in three of four control positions (in correspondence with sensors 2, 8 and 11); reconstruction results on sensor 10 are not as good as the others, but better than those observed with the other layouts. Generally speaking, Table 4 clearly shows that L2 and L3 produce the best results (i.e., the lower reconstruction errors), but L3 shows the best performance on sensor 8 position, probably thanks to the presence of two reconstruction sensors on the left side which is the first to reach the water surface with this wedge inclination. Generally speaking, an improvement in the reconstruction of the strain is detected in comparison with the $0°$ V–$0°$ G impact; this is probably related to the variation in the impact dynamics which provides for the water entry of the left bottom side of the wedge before than the right bottom side, in particular related to the first timesteps after the water impact.
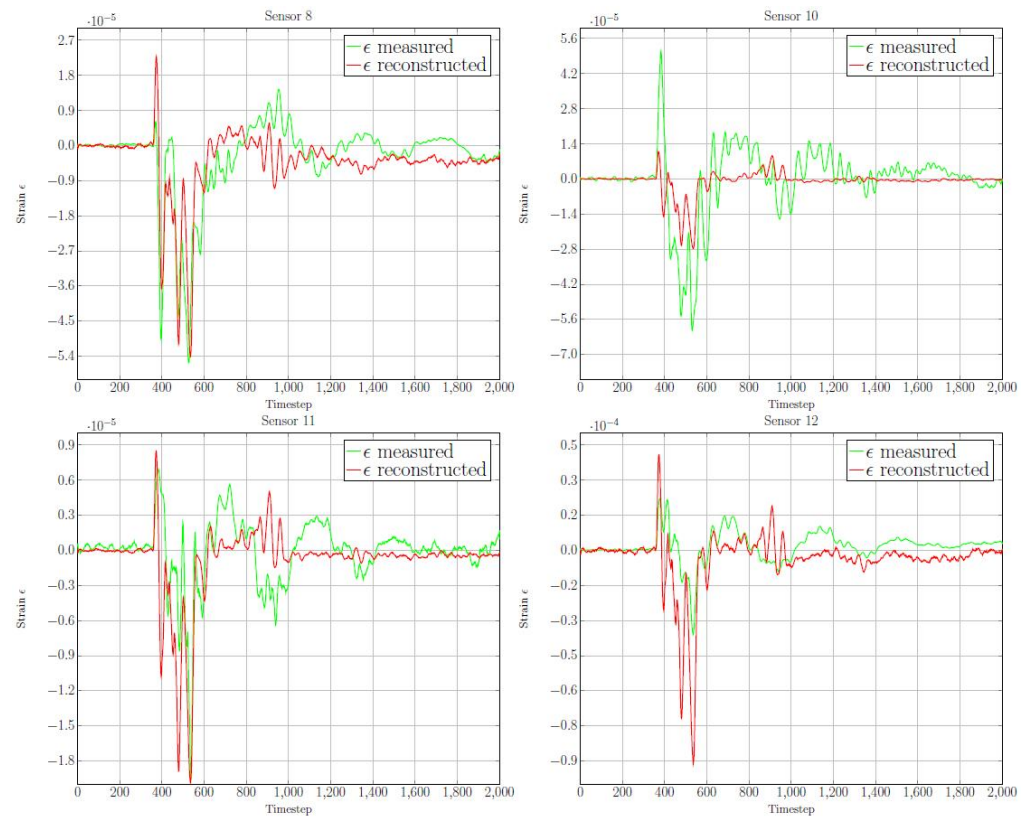
Figure 9. 0° V–10° G impact test—Layout 1 measured vs. reconstructed strain signals.
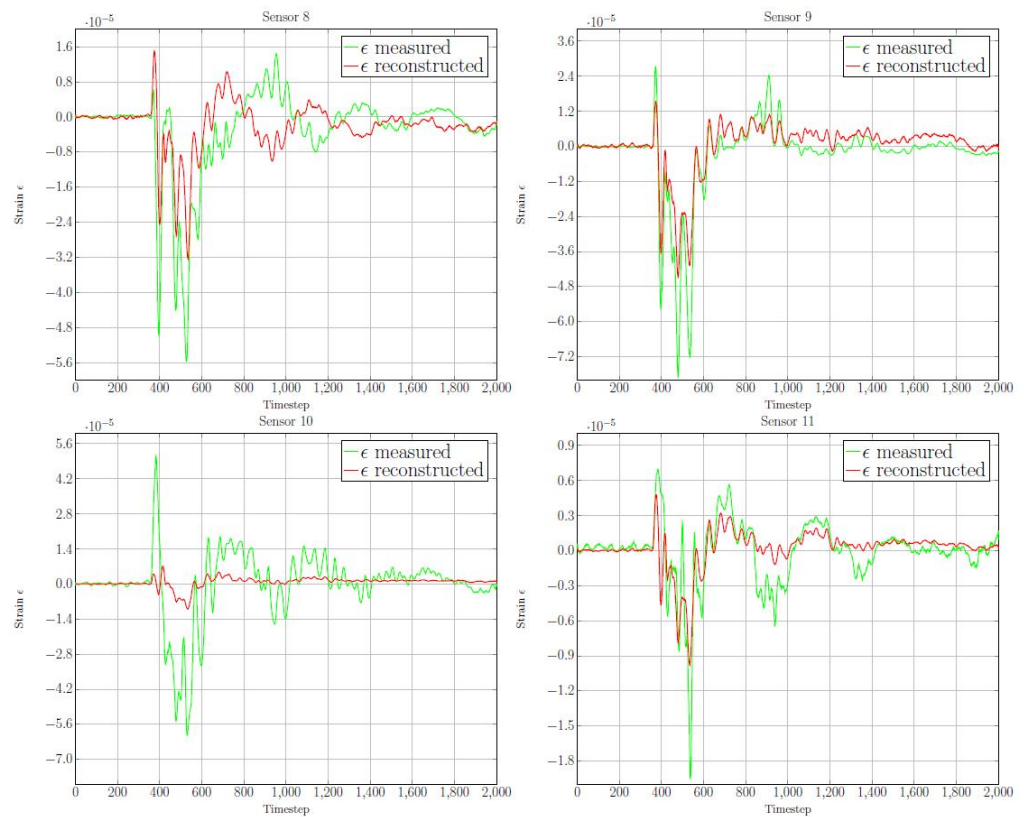

Figure 10. 0° V–10° G impact test—Layout 2 measured vs. reconstructed strain signals.
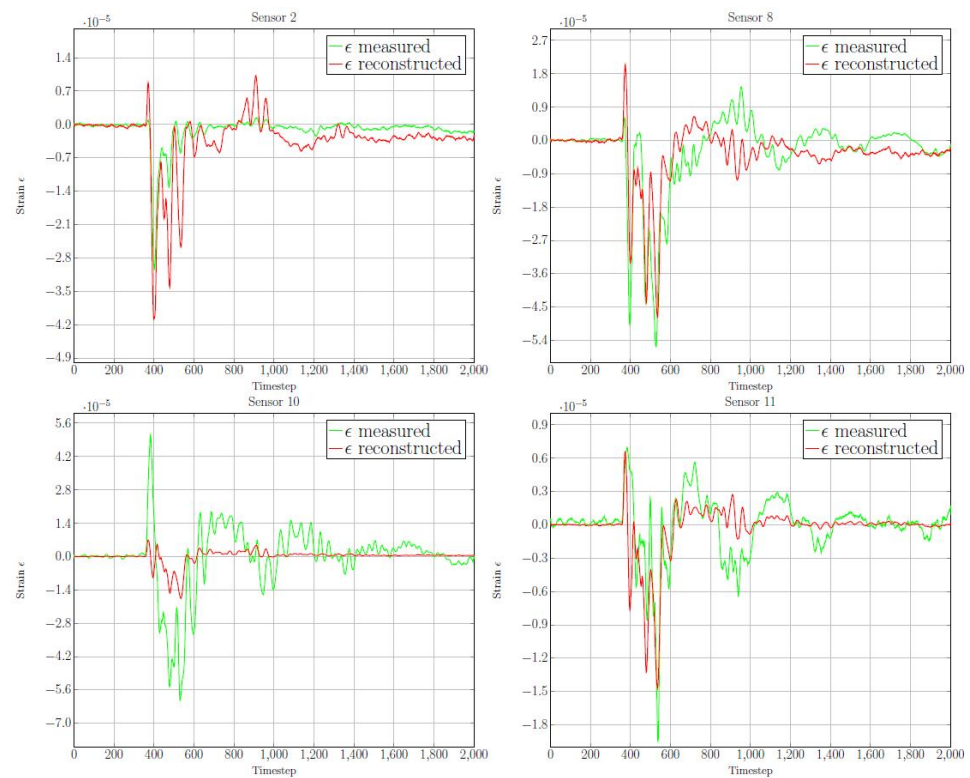
Figure 11. $0°$ V–$10°$ G impact test—Layout 3 measured vs. reconstructed strain signals.

Table 5. $0°$ V–$10°$ G impact test—Layout reconstruction errors E_n for each control sensor.

Layout	Control Sensors	Error on CS 1	Error on CS 2	Error on CS 3	Error on CS 4
L1	8-10-11-12	0.096	0.132	0.096	0.197
L2	8-9-10-11	0.107	0.052	0.130	0.067
L3	2-8-10-11	0.085	0.096	0.130	0.076

5.3. $10°$ V–$0°$ G Impact

The third impact test is identified by $10°$ V–$0°$ G impact angle, set through an anti-clockwise rotation of the rail with respect to the vertical direction, and drop height of 0.5 m. The comparisons between reconstructed and measured strain signals on the control sensors positions for each layout are shown in Figures 12–14. Table 6 summarizes the related E_n error values. Layout 1 results feature an appreciable reconstruction quality on all the control positions, taking into account the presence of unconformities in terms of amplitude in correspondence with the first impact timesteps. It is also interesting to note that the sensor 10 signal seems to be better reconstructed than in the previous two tests. Considering that the same drop height and reconstruction sensors have been used, this confirms the correlation of the reconstruction quality with the impact angle, in this test related to the free-fall velocity angle set through the impact setup. Layout 2 results are slightly different. We observe a better performance considering sensor 11 position and substantially the same for sensor 8 position (see Table 5), while on sensor 10 position, despite an improvement with respect to previous tests, a slightly worse reconstruction than L1 one is detected. Sensor 9 position is featured by a good agreement, but the first peaks after the impact are not reconstructed with the same amplitude of the measured signal. Layout 3 shows results similar to Layout 1, e.g., on sensor 8 and sensor 10 control positions; moreover, a better reconstruction is achieved on sensor 11 position, probably for the presence of sensor 12 in the reconstruction layout. For all the layouts, the reconstruction on sensor 8 position is not as good as in $10°$V-$0°$G test, probably because of the differences in the water pressure field on sensor 8 bottom side in the inclined velocity fall. Also in this case, Layout 3 performance is

positively influenced by the distribution of reconstruction sensors, which allows to reach the best quality in reconstruction considering all the control locations on the rib.
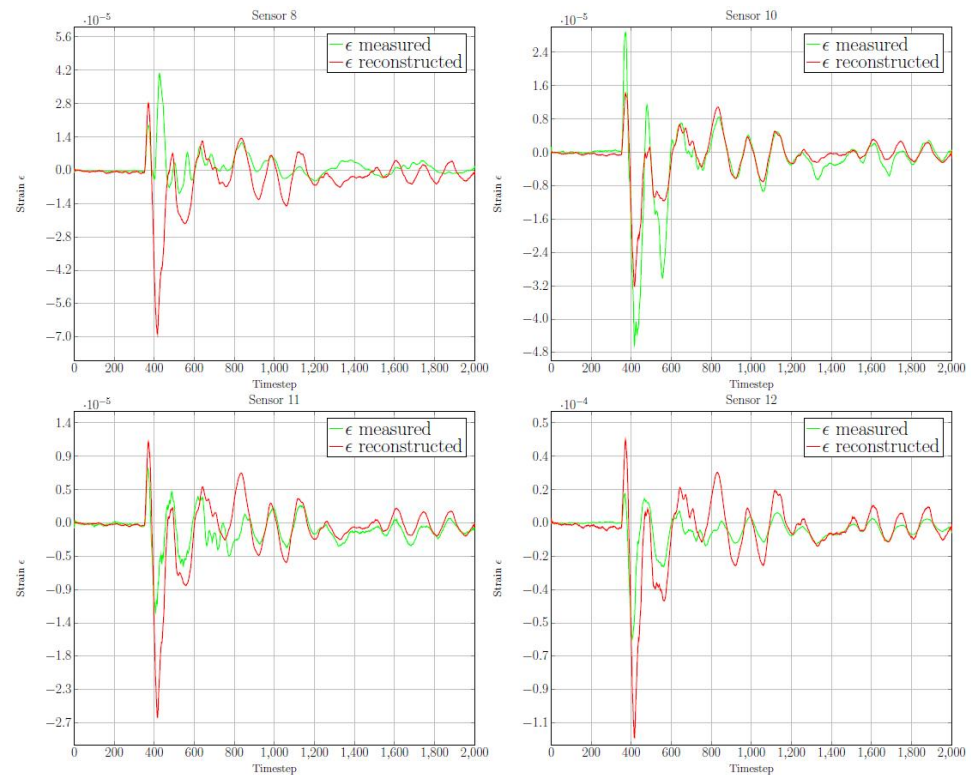

Figure 12. 10° V–0° G impact test—Layout 1 measured vs. reconstructed strain signals.
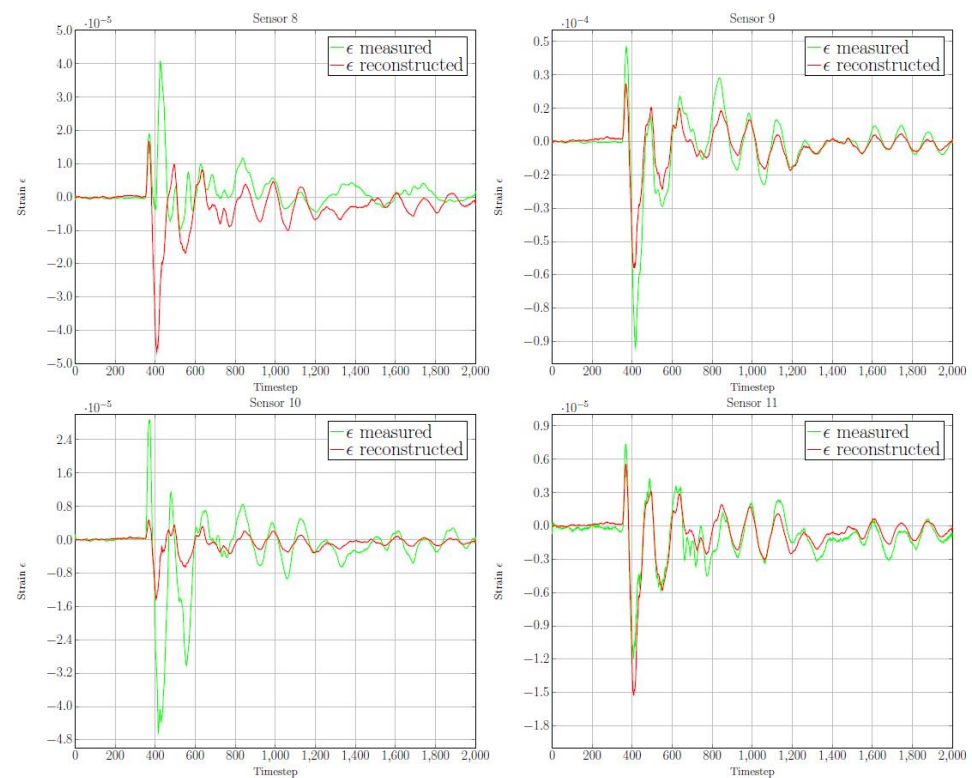

Figure 13. 10° V–0° G impact test—Layout 2 measured vs. reconstructed strain signals.
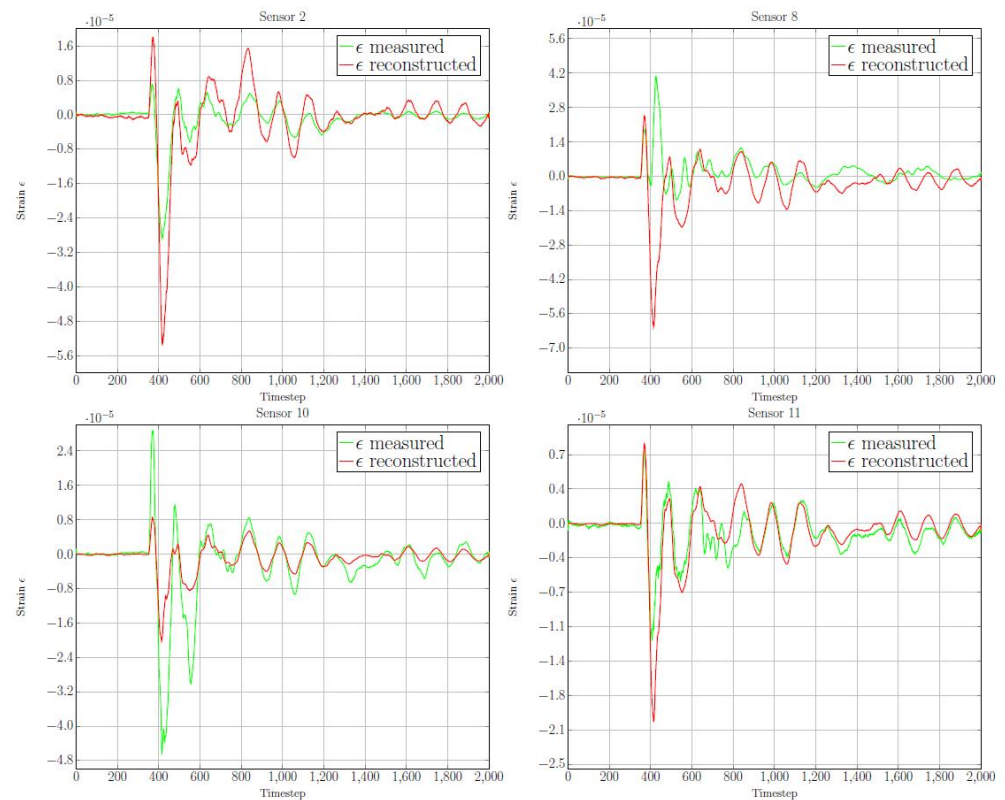
Figure 14. $10°$ V – $0°$ G impact test—Layout 3 measured vs. reconstructed strain signals.

Table 6. $10°$ V–$0°$ G impact test—Layout reconstruction errors E_n for each control sensor.

Layout	Control Sensors	Error on CS 1	Error on CS 2	Error on CS 3	Error on CS 4
L1	8-10-11-12	0.077	0.103	0.119	0.150
L2	8-9-10-11	0.085	0.034	0.109	0.078
L3	2-8-10-11	0.036	0.077	0.106	0.094

6. Discussion

Experimental results in terms of reconstruction error clearly confirm the potential of the presented method for strain reconstruction considering a proper choice of the reconstruction layout (e.g., Layout 3 in this work); the low values of E_n of Layout 3 reconstructed signals assess the closeness to measured strain signal, which will make possible further works focused on the comparison between strain signals reconstructed on damaged and undamaged structures, for the evaluation of the methodology for structural health monitoring. Moreover, results lead to the following specific conclusions on reconstruction layouts features: (i) a homogeneous distribution of reconstruction sensors along the structure (like Layout 3) allows a higher quality reconstruction both on near-keel and far-keel positioned sensors by computing the modal coordinates from strain signal which are not so far from the control positions; (ii) the reconstruction quality on near-keel sensors is better in case of oblique impact, because of the variation in the impact pressure related to the water entry of the left bottom side of the wedge before than the right bottom side both for V $\neq 0°$ tests and for G $\neq 0°$ tests. This allows an improvement in the reconstruction of the strain related to the first timesteps after the water impact thanks to the presence of reconstruction sensors close to the keel. Furthermore, it must be considered that the keel is more rigid than other ship hull zone, which makes keel strain reconstruction harder than others; (iii) the reconstruction of strain on sensor 8 position in the V $= 10°$/G $= 0°$ test is not as good as in the V $= 0°$/G $= 10°$ test, probably because of a different distribution of the water pressure

field on the wedge left bottom side between a wedge-inclined free fall and an inclined velocity fall. More generally, the achieved results can be considered satisfactory in terms of signal amplitude and effectiveness in reconstructing both compression and traction strain; furthermore, there is an appreciable correspondence between reconstructed and measured signals in the first strain peaks after the impact and in signal frequencies.

7. Conclusions

The results presented in this paper confirm the effectiveness of the proposed methodology to reconstruct the structural behaviour of flexible bodies impacting on water free surface. Our analysis provides an extension of this methodology to 3D wedge geometries. This method, based on previous works of the same research path, provides for the application of the modal decomposition method on local strain signal from FBG sensors installed on the specimen to reconstruct the mechanical behaviour of the body during the interaction with water, typical of impacts on the free surface, in the case of vertical and oblique free falls. In order to evaluate the reconstruction quality, installed sensors were divided into reconstruction sensors, (employed to achieve the modal coordinates and, consequently, to compute the strain and displacement), and control sensors. At the control sensor locations, the strain values can be reconstructed and compared with the strain signal acquired by control sensors themselves, in order to check the reconstruction's effectiveness. An experimental campaign was carried out to achieve a concrete assessment of the methodology. In particular, we analysed the water impact of an aluminium wedge modified to reach a geometry similar to ship hulls by means of a welded central thin plate, acting as the hull rib. The wedge was released from a height of 0.5 m with different slopes of both the velocity vector (modified through the rotation of the rail on which the specimen carriage system translates) and the wedge, represented by the V and the G angles respectively. Modal displacement and strain normalized components at the measurement locations were calculated through a finite element model of the specimen. A modal analysis allowed the matrices to be gathered through the choice of the most suited modes for reconstruction purposes on the rib. Twelve FBG sensors were installed on the rib; eight of them were chosen as reconstruction sensors, the other four as control sensors [7]. Overall, the reconstruction method has shown its potential in strain field reconstruction in case of vertical and oblique impacts of flexible wedges; this work confirms the potential of the presented methodology for achieving appreciable reconstruction of the structural behaviour of bodies impacting water, which can be considered a reliable basis for damage detection and localization purposes.

Author Contributions: Conceptualization, S.U., P.F.; E.J. and C.B.; methodology, P.F. and G.F.; software, P.F. and A.M.; investigation, G.F. and A.M.; writing—original draft preparation, A.M. and C.B.; writing—review and editing, all authors; supervision, E.J. and S.U.; project administration, C.B.; funding acquisition, C.B., P.F. and G.F. All authors have read and agreed to the published version of the manuscript.

References

1. Abrate, S. Hull Slamming. *Appl. Mech. Rev.* **2011**, *64*, 060803. [CrossRef]
2. Charca, S.; Shafiq, B.; Just, F. Repeated Slamming of Sandwich Composite Panels on Water. *J. Sandw. Struct. Mater.* **2009**, *11*, 409–424. [CrossRef]
3. Yamamoto, Y.; Iida, K.; Fukasawa, T.; Murakami, T.; Arai, M.; Ando, A. Structural Damage Analysis of a Fast Ship Due to Bow Flare Slamming. *Int. Shipbuild. Prog.* **1985**, *32*, 124–136. [CrossRef]
4. Seddon, C.; Moatamedi, M. Review of Water Entry with Applications to Aerospace Structures. *Int. J. Impact Eng.* **2006**, *32*, 1045–1067. [CrossRef]

5. Panciroli, R.; Ubertini, S.; Minak, G.; Jannelli, E. Experiments on the Dynamics of Flexible Cylindrical Shells Impacting on a Water Surface. *Exp. Mech.* **2015**, *55*, 1537–1550. [CrossRef]

6. Fanelli, P.; Biscarini, C.; Jannelli, E.; Ubertini, F.; Ubertini, S. Structural Health Monitoring of Cylindrical Bodies under Impulsive Hydrodynamic Loading by Distributed FBG Strain Measurements. *Meas. Sci. Technol.* **2017**, *28*, 024006. [CrossRef]

7. Mercuri, A.; Fanelli, P.; Ubertini, S.; Falcucci, G.; Jannelli, E.; Biscarini, C. Effect of Strain Measurement Layout on Damage Detection and Localization in a Free Falling Compliant Cylinder Impacting a Water Surface. *Fluids* **2021**, *6*, 58. [CrossRef]

8. Panciroli, R.; Biscarini, C.; Falcucci, G.; Jannelli, E.; Ubertini, S. Live Monitoring of the Distributed Strain Field in Impulsive Events through Fiber Bragg Gratings. *J. Fluids Struct.* **2016**, *61*, 60–75. [CrossRef]

9. Fanelli, P.; Facci, A.L.; Russo, S. Influence of Sensors Layout in Damage Monitoring of Cylindrical Bodies under Impulsive Hydrodynamic Loading. *AIP Conf. Proc.* **2018**, *1978*, 420009.

10. Fanelli, P.; Trupiano, S.; Belardi, V.G.; Vivio, F.; Jannelli, E. Structural Health Monitoring Algorithm Application to a Powerboat Model Impacting on Water Surface. *Procedia Struct. Integr.* **2019**, *24*, 926–938. [CrossRef]

11. Fanelli, P.; Facci, A.; Jannelli, E. Live Crack Damage Detection with Local Strain Measurement on Solid Bodies Subjected to Hydrodynamic Loading. *Procedia Struct. Integr.* **2018**, *8*, 539–551. [CrossRef]

12. Kang, L.-H.; Kim, D.-K.; Han, J.-H. Estimation of Dynamic Structural Displacements Using Fiber Bragg Grating Strain Sensors. *J. Sound Vib.* **2007**, *305*, 534–542. [CrossRef]

13. Bogert, P.; Haugse, E.; Gehrki, R. Structural Shape Identification from Experimental Strains Using a Modal Transformation Technique. In Proceedings of the 44th AIAA/ASME/ASCE/AHS/ASC Structures, Structural Dynamics, and Materials Conference, Norfolk, Virginia, 7–10 April 2003; p. 1898.

14. Kashyap, R. *Fiber Bragg Gratings*; Elsevier: San Diego, CA, USA, 1999; ISBN 9780124005600.

15. Grattan, K.T.V.; Sun, T. Fiber Optic Sensor Technology: An Overview. *Sensors Actuators A Phys.* **2000**, *82*, 40–61. [CrossRef]

16. Silva-Muñoz, R.A.; Lopez-Anido, R. Structural Health Monitoring of Marine Composite Structural Joints Using Embedded Fiber Bragg Grating Strain Sensors. *Compos. Struct.* **2009**, *89*, 224–234. [CrossRef]

17. Kuang, K.; Kenny, R.; Whelan, M.; Cantwell, W.; Chalker, P. Embedded Fibre Bragg Grating Sensors in Advanced Composite Materials. *Compos. Sci. Technol.* **2001**, *61*, 1379–1387. [CrossRef]

18. Guemes, J.; Menéndez, J. Response of Bragg Grating Fiber-Optic Sensors When Embedded in Composite Laminates. *Compos. Sci. Technol.* **2002**, *62*, 959–966. [CrossRef]

19. And, K.K.; Cantwell, W.; Kuang, K.S.C.; Cantwell, W. Use of Conventional Optical Fibers and Fiber Bragg Gratings for Damage Detection in Advanced Composite Structures: A Review. *Appl. Mech. Rev.* **2003**, *56*, 493–513. [CrossRef]

20. Fanelli, P.; Mercuri, A.; Trupiano, S.; Vivio, F.; Falcucci, G.; Jannelli, E. Live Reconstruction of Global Loads on a Powerboat Using Local Strain FBG Measurements. *Procedia Struct. Integr.* **2019**, *24*, 949–960. [CrossRef]

21. Russo, S.; Biscarini, C.; Facci, A.L.; Falcucci, G.; Jannelli, E.; Ubertini, S. Experimental Assessment of Buoyant Cylinder Impacts through High-Speed Image Acquisition. *J. Mar. Sci. Technol.* **2018**, *23*, 67–80. [CrossRef]

22. Faltinsen, O.; Kjærland, O.; Nøttveit, A.; Vinje, T. Water Impact Loads And Dynamic Response Of Horizontal Circular Cylinders In Offshore Structures. In Proceedings of the Offshore Technology Conference, Houston, TX, USA, 1–4 May 1977.

23. Khabakhpasheva, T. Fluid–Structure Interaction during the Impact of a Cylindrical Shell on a Thin Layer of Water. *J. Fluids Struct.* **2008**, *25*, 431–444. [CrossRef]

24. Lin, M.-C.; Shieh, L.-D. Flow Visualization and Pressure Characteristics of a Cylinder for Water Impact. *Appl. Ocean Res.* **1997**, *19*, 101–112. [CrossRef]

25. Sun, H.; Faltinsen, O.M. Water Impact of Horizontal Circular Cylinders and Cylindrical Shells. *Appl. Ocean Res.* **2006**, *28*, 299–311. [CrossRef]

26. Van Nuffel, D.; Vepa, K.; De Baere, I.; Lava, P.; Kersemans, M.; Degrieck, J.; De Rouck, J.; VAN Paepegem, W. A Comparison between the Experimental and Theoretical Impact Pressures Acting on a Horizontal Quasi-Rigid Cylinder during Vertical Water Entry. *Ocean Eng.* **2014**, *77*, 42–54. [CrossRef]

27. Wei, Z.; Hu, C. An Experimental Study on Water Entry of Horizontal Cylinders. *J. Mar. Sci. Technol.* **2014**, *19*, 338–350. [CrossRef]

28. Wei, Z.; Hu, C. Experimental Study on Water Entry of Circular Cylinders with Inclined Angles. *J. Mar. Sci. Technol.* **2015**, *20*, 722–738. [CrossRef]

29. Facci, A.L.; Falcucci, G.; Agresta, A.; Biscarini, C.; Jannelli, E.; Ubertini, S. Fluid Structure Interaction of Buoyant Bodies with Free Surface Flows: Computational Modelling and Experimental Validation. *Water* **2019**, *11*, 1048. [CrossRef]

30. Falcucci, G.; Amati, G.; Fanelli, P.; Krastev, V.K.; Polverino, G.; Porfiri, M.; Succi, S. Extreme Flow Simulations Reveal Skeletal Adaptations of Deep-Sea Sponges. *Nat. Cell Biol.* **2021**, *595*, 537–541. [CrossRef]

31. Shams, A.; Zhao, S.; Porfiri, M. Hydroelastic Slamming of Flexible Wedges: Modeling and Experiments from Water Entry to Exit. *Phys. Fluids* **2017**, *29*, 037107. [CrossRef]

32. Russo, S.; Jalalisendi, M.; Falcucci, G.; Porfiri, M. Experimental Characterization of Oblique and Asymmetric Water Entry. *Exp. Therm. Fluid Sci.* **2018**, *92*, 141–161. [CrossRef]